

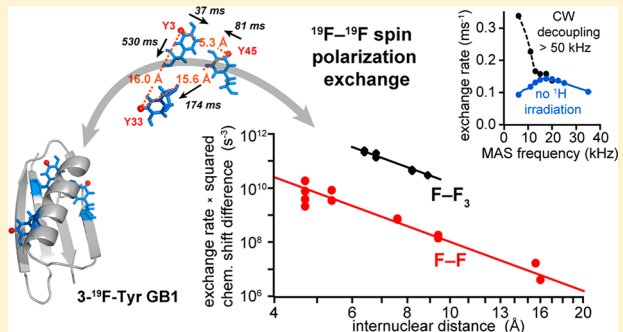
Fast Magic-Angle-Spinning ^{19}F Spin Exchange NMR for Determining Nanometer ^{19}F – ^{19}F Distances in Proteins and Pharmaceutical Compounds

Matthias Roos,¹ Tuo Wang,¹ Alexander A. Shcherbakov,¹ and Mei Hong^{*1,2}

Department of Chemistry, Massachusetts Institute of Technology, 170 Albany Street, Cambridge, Massachusetts 02139, United States

Supporting Information

ABSTRACT: Internuclear distances measured using NMR provide crucial constraints of three-dimensional structures but are often restricted to about 5 Å due to the weakness of nuclear-spin dipolar couplings. For studying macromolecular assemblies in biology and materials science, distance constraints beyond 1 nm will be extremely valuable. Here we present an extensive and quantitative analysis of the feasibility of ^{19}F spin exchange NMR for precise and robust measurements of interatomic distances up to 1.6 nm at a magnetic field of 14.1 T, under 20–40 kHz magic-angle spinning (MAS). The measured distances are comparable to those achievable from paramagnetic relaxation enhancement but have higher precision, which is better than ± 1 Å for short distances and ± 2 Å for long distances. For ^{19}F spins with the same isotropic chemical shift but different anisotropic chemical shifts, intermediate MAS frequencies of 15–25 kHz without ^1H irradiation accelerate spin exchange. For spectrally resolved ^{19}F – ^{19}F spin exchange, ^1H – ^{19}F dipolar recoupling significantly speeds up ^{19}F – ^{19}F spin exchange. On the basis of data from five fluorinated synthetic, pharmaceutical, and biological compounds, we obtained two general curves for spin exchange between CF groups and between CF_3 and CF groups. These curves allow ^{19}F – ^{19}F distances to be extracted from the measured spin exchange rates after taking into account ^{19}F chemical shifts. These results demonstrate the robustness of ^{19}F spin exchange NMR for distance measurements in a wide range of biological and chemical systems.



INTRODUCTION

Interatomic distances represent the most important constraints in three-dimensional structure determination by NMR. Although short-range distances (<5 Å) can be precisely measured using a variety of NMR experiments, long-range distances between well separated segments in biomolecules are more challenging to measure but are crucial constraints of the three-dimensional folds of proteins and other macromolecules.¹ For oligomeric systems such as α -helical bundles, β -barrels, and cross- β fibrils, intermolecular distances over 1 nm are invaluable for determining the structures of the intermolecular interfaces.

Magic-angle-spinning (MAS) NMR has been used extensively to measure distances in insoluble and noncrystalline biomolecules and organic compounds.^{2–4} The most common solid-state NMR (SSNMR) approach for distance measurements is to detect ^{13}C – ^{13}C cross peaks in 2D or 3D correlation spectra as a semiquantitative indicator of interatomic distances.^{5–7} These ^{13}C – ^{13}C cross peaks are commonly measured using spin diffusion techniques based on second-order recoupling, such as proton-driven spin diffusion (PDSD),⁸ dipolar-assisted rotational resonance or RF assisted spin diffusion (DARR/RAD),^{9,10} proton-assisted recoupling (PAR),¹¹ second-order Hamiltonian among analogous nuclei generated by heteronuclear assistance irradiation (SHANGHAI) and its analogs,^{12–14} and combined $R2_{\text{n}}^{\text{v}}$ -driven spin diffusion

(CORD).¹⁵ Although these second-order recoupling techniques have become increasingly more robust with respect to isotropic chemical-shift differences and fast MAS in high magnetic fields, the upper limit of measurable ^{13}C – ^{13}C distances is still fundamentally limited by the low ^{13}C gyromagnetic ratio, which weakens the ^{13}C – ^{13}C dipolar coupling, to about 7–8 Å.¹⁶ Further, for uniformly ^{13}C -labeled proteins, even independent of dipolar truncation,¹⁷ relayed polarization transfer involving three or more ^{13}C spins remains much more efficient than direct polarization transfer, which makes ^{13}C – ^{13}C cross peaks sensitive to the geometry of the local spin network and less accurately reflecting the long-range ^{13}C – ^{13}C distance of interest. Finally, for organic and pharmaceutical compounds that are not readily amenable to ^{13}C labeling, ^{13}C – ^{13}C distance measurements have very low sensitivity due to the 1.1% natural abundance of ^{13}C , unless sensitivity enhancement techniques such as dynamic nuclear polarization (DNP) are employed.¹⁸

Compared to homonuclear distances, heteronuclear distances can be measured quantitatively using REDOR¹⁹ and other recoupling techniques,²⁰ with the ^{13}C – ^{15}N distance being the most commonly measured distances in protein structure

Received: January 10, 2018

Revised: February 23, 2018

Published: February 27, 2018

Table 1. ^{19}F Chemical-Shift Tensor Parameters of the Compounds Studied in This Work^a

compounds	sites	δ_{iso} (ppm)	$\Delta\delta = \delta_{zz} - \delta_{\text{iso}}$ (ppm)	η
5F-Trp	$\text{S}-^{19}\text{F}$	-122.1	53.7 ± 0.8	0.04 ± 0.08
PNC	F_N	-113.4	-89.1 ± 2.2	0.52 ± 0.04
	F_P	-118.9	-75.9 ± 0.9	0.42 ± 0.06
	F_O	-104.8	77.2 ± 0.2	0.80 ± 0.06
sitagliptin	F_M	-137.8	-77.8 ± 2.7	0.51 ± 0.01
	F_P	-147.1	-74.2 ± 1.6	0.47 ± 0.04
	F_O	-116.0	-74.9 ± 1.0	0.78 ± 0.01
	CF_3	-66.0	35.2 ± 2.3	0.03 ± 0.04
formyl-MLF	F_P	-116.1	58.0 ± 0.8	0.94 ± 0.02
	CF_3	-38.9	19.3 ± 0.4	0.85 ± 0.03
GB1	$3\text{-}^{19}\text{F}-\text{Y3}$	-133.3	-76 ± 3	0.4 ± 0.2
	$3\text{-}^{19}\text{F}-\text{Y33}$	-135.9	-56.2 ± 0.7	0.2 ± 0.2
	$3\text{-}^{19}\text{F}-\text{Y45}$	-132.9	-75 ± 1	0.4 ± 0.1

^aChemical-shift anisotropies are obtained from Herzfeld–Berger analysis.⁶²

determination. However, the ^{15}N gyromagnetic ratio is even lower than that of ^{13}C , so that $^{13}\text{C}-^{15}\text{N}$ distances cannot be measured beyond ~ 5 Å. Paramagnetic relaxation enhancement (PRE) NMR represents a third class of approach that can access much longer distances by making use of unpaired electron spins that enhance nuclear T_1 or T_2 relaxation in a distance-dependent manner.²¹ Because of the 2–3 orders of magnitude larger electron gyromagnetic ratio over nuclear gyromagnetic ratios, distances up to ~ 20 Å can be measured from PRE effects.^{22–26} However, paramagnetic dipolar relaxation does not give as precise distances as direct dipolar couplings and requires either endogenous paramagnetic centers or incorporation of paramagnetic tags at carefully chosen locations that do not perturb protein structures.²⁷ Therefore, distance measurement for high-resolution biomolecular structure determination by NMR is still largely limited to subnanometer distances.

^{19}F NMR has long been recognized as having several major advantages for structure determination. First, ^{19}F is absent in naturally occurring biomolecules; thus synthetic and biosynthetic incorporation of fluorine into biomolecules provides site-specific probes of molecular structures without a background signal. Fluorine incorporation also causes much less structural perturbation than paramagnetic additives or fluorescent labels,^{28–30} because fluorine has a van der Waals radius that is similar to that of ^1H . Second, ^{19}F spins have large isotropic and anisotropic chemical shifts; thus they are extremely sensitive to the chemical structure and conformational structure of molecules. Third, ^{19}F is 100% abundant and has a gyromagnetic ratio that is almost as high (94%) as that of ^1H . Thus, ^{19}F NMR has extremely high sensitivity. For these reasons, ^{19}F NMR has become increasingly adopted in biomolecular structure determination, especially for challenging systems such as membrane-bound G-protein coupled receptors.^{31–33} Finally, fluorine is already incorporated in more than $\sim 20\%$ of pharmaceutical compounds because of its favorable chemical properties,^{30,34} which makes ^{19}F NMR a natural probe of protein–drug and protein–ligand interactions.

One benefit of the high ^{19}F gyromagnetic ratio is the strong $^{19}\text{F}-^{19}\text{F}$ dipolar coupling: for the same distances, $^{19}\text{F}-^{19}\text{F}$ dipolar couplings are 14-fold stronger than $^{13}\text{C}-^{13}\text{C}$ dipolar couplings; conversely, for the same dipolar couplings, $^{19}\text{F}-^{19}\text{F}$ distances are 2.4-fold longer than $^{13}\text{C}-^{13}\text{C}$ distances, suggesting that $^{19}\text{F}-^{19}\text{F}$ distances up to ~ 19 Å, as compared to $^{13}\text{C}-^{13}\text{C}$ distances up to ~ 8 Å, may be measurable. Indeed, polarization transfer between fluorine spins with the same isotropic chemical

shift but different anisotropic chemical shifts has been exploited using the CODEX technique³⁵ to measure intermolecular distances in homo-oligomeric protein assemblies.^{36–42} This ^{19}F “anisotropy spin exchange” has so far been mainly utilized at moderate magnetic fields such as 9.4 T (corresponding to a ^{19}F Larmor frequency of 376 MHz), where the ^{19}F chemical-shift anisotropy (CSA) is not very large. Under this condition, low MAS frequencies of ~ 10 kHz can be employed to avoid slowing down $^{19}\text{F}-^{19}\text{F}$ spin diffusion. However, low magnetic fields reduce the sensitivity of the experiment and compromise the resolution of chemically distinct ^{19}F spins. To date, only a small number of studies have explored spectrally resolved $^{19}\text{F}-^{19}\text{F}$ distance measurements in small molecules,⁴³ fluorinated polymers,⁴⁴ and inorganic fluorides.^{45–47} These studies have been mostly conducted at moderate magnetic fields, focused on distances of < 1 nm and did not consider the effects of the ^{19}F chemical shifts on the accuracy of distance extraction.

Here we present a systematic exploration of the accurate measurement of $^{19}\text{F}-^{19}\text{F}$ distances up to 1.6 nm at a magnetic field of 14.1 T under 20–40 kHz MAS. We demonstrate zero-quantum ^{19}F spin polarization exchange in organic molecules, pharmaceutical compounds, peptides, and proteins that contain both trifluoromethyl groups and aromatic fluorines. We consider both anisotropy spin exchange observed in 1D ^{19}F NMR spectra and spectrally resolved spin exchange in 2D $^{19}\text{F}-^{19}\text{F}$ correlation spectra. For exchange between ^{19}F spins with the same isotropic chemical shift but different anisotropic shifts, we investigated the optimal ^1H irradiation condition and MAS frequency regime and show that anisotropy spin exchange can be *faster* under fast MAS than under slow MAS, in contrast to common expectation. For spectrally resolved spin exchange, we show that 2D $^{19}\text{F}-^{19}\text{F}$ correlation experiments can yield distances with quantifiable dependence on chemical shifts. We identified two master curves, one for CF_3-F and the other for $\text{F}-\text{F}$, which relate the polarization transfer rates to $^{19}\text{F}-^{19}\text{F}$ distances. These results promise a robust and high-sensitivity NMR approach for measuring distance constraints in proteins and pharmaceutical compounds.

MATERIALS AND METHODS

Preparation of Fluorinated Compounds. Five fluorinated compounds are used in this study (Table 1). 5- ^{19}F -L-tryptophan (5F-Trp), 7-chloro-1-(2,4-difluorophenyl)-6-fluoro-4-oxo-1,4-dihydro[1,8]naphthyridine-3-carboxylic acid (PNC), and sitagliptin phosphate ($\text{C}_{16}\text{H}_{15}\text{F}_6\text{N}_5\text{O}\cdot\text{H}_3\text{PO}_4\cdot\text{H}_2\text{O}$) were purchased

from Sigma-Aldrich. Formyltrifluoromethionine-¹³C, ¹⁵N-leucine-*p*-¹⁹F-phenylalanine (formyl-MLF) was custom-synthesized by Biopeptek Pharmaceuticals (Malvern, PA).

SF-Trp was studied as a dry neat powder, whereas PNC, sitagliptin and formyl-MLF were diluted with cosolutes at a 1:5 or 1:6 mass ratio to avoid intermolecular polarization transfer. PNC and unlabeled Trp at 1:5 mass ratio were codissolved in a 1:3 2-propanol–water solution at 60 °C and sonicated until complete dissolution. Sitagliptin was dissolved in water and mixed with unlabeled Trp at a 1:6 mass ratio, briefly heated up to 80 °C and sonicated. Formyl-MLF was dissolved in acetic acid and mixed with nonfluorinated formyl-MLF at a 1:6 mass ratio at 60 °C, again with sonication. After complete dissolution, each sample was rapidly frozen in liquid nitrogen and lyophilized, giving homogeneous powders that were packed into 1.9 mm MAS rotors. Freeze-drying was used instead of cocrystallization to avoid self-association and clustering of the fluorinated compounds and to prevent precipitation of the compound with lower solubility upon increasing solute concentration.

3-¹⁹F-Tyr labeled GB1 (3-Tyr-GB1) was expressed in BL21 (DE3) *E. coli* cells containing GB1 plasmids that were cultured on ampicillin-containing LB agar. A single colony was used to inoculate 10 mL of LB for 12–14 h at 37 °C. A 5.0 mL aliquot of the cultured bacteria was transferred to 500 mL of unlabeled (¹²C, ¹⁴N) M9 media (48.1 mM Na₂HPO₄, 22.0 mM KH₂PO₄, 8.56 mM NaCl, 2.00 mM MgSO₄, 0.100 mM CaCl₂, 1.00 g/L NH₄Cl, 2.00 g/L glucose, 100 µg/mL ampicillin) and was allowed to grow to OD₆₀₀ = 0.4. Samples (50 mg) of unlabeled L-phenylalanine, L-tryptophan, and 3-fluoro-L-tyrosine were dissolved in 5 mL of M9 media at 50 °C. The cells were then spun down at 7000 rpm and 25 °C for 10 min. The pellet was resuspended in 500 mL of M9 media containing ¹⁵NH₄Cl and ¹³C-glucose. Glyphosate was added to a final concentration of 1 g/L after 30 min and the temperature was changed to 28 °C; unlabeled L-phenylalanine, L-tryptophan, and 3-fluoro-L-tyrosine solutions were added to the culture simultaneously with glyphosate addition. When OD₆₀₀ reached 0.6, isopropyl β-D-thiogalactoside (IPTG) was added to a concentration of 0.5 mM to induce protein expression for 5–6 h. The cells were spun down at 7000 rpm and 4 °C for 15 min, and the bacterial pellet was resuspended in 50 mL of lysis buffer (200 mM NaCl, 50 mM KH₂PO₄/K₂HPO₄, pH 7). The suspension was heated in a water bath at 80 °C for 5 min and then chilled on ice for 15 min. The mixture was centrifuged at 16000g and 4 °C for 1 h to pellet insoluble cell matter. The supernatant was concentrated to ~10 mL using Amicon Ultra-15 3000 Da molecular weight cutoff (MWCO) centrifugal concentrators (Millipore). The protein was purified by size-exclusion chromatography using a HiLoad 26/60 Superdex 75 prep grade column (GE) using a 50 mM KH₂PO₄/K₂HPO₄, 100 mM NaCl buffer at pH 7.0. The yield of the purified protein was determined by UV-vis at 280 nm to be 50 mg from 500 mL of culture. The purified protein solution was dialyzed against 4 L of 50 mM KH₂PO₄/K₂HPO₄ buffer at pH 5.5 to remove NaCl. The dialysis buffer was changed twice a day for 4 days. Microcrystalline protein was obtained by mixing 1 mL of 30 mg/mL GB1 solution with three 1 mL aliquots of crystallizing solution containing 2-methyl-2,4-pentanediol (MPD) and isopropanol (IPA) at a volume ratio of 2:1. The microcrystalline protein was packed into a 1.9 mm MAS rotor containing two silicone antidehydration spacers between the end-caps and the rotor body. About 12 mg of GB1 microcrystals and organic solution was packed into the rotor.

The fluoro-tyrosine incorporation level was determined to be 95% using ESI and MALDI-TOF mass spectrometry.

Solid-State NMR Experiments. Solid-state NMR experiments were conducted on a Bruker Avance III HD spectrometer operating at a magnetic field of 14.1 T and a ¹⁹F Larmor frequency of 564.66 MHz. A 1.9 mm MAS HFX probe with a maximum MAS frequency of 42 kHz was used. ¹⁹F chemical shifts were referenced to the -122.1 ppm chemical shift of SF-Trp on the CF₃Cl scale.³⁷ 2D ¹⁹F-¹⁹F correlation spectra were measured under 25 kHz MAS. CODEX experiments on SF-Trp were conducted from 6 kHz to 35 kHz MAS to investigate the dependence of spin exchange on MAS frequency. Sample temperature was maintained at ~300 K by adjusting the temperature set point such that the MAS frictional heating effects are compensated.⁴⁸

For SF-Trp, PNC, and GB1, ¹H-¹⁹F cross-polarization (CP) was used to avoid long recycle delays due to the long ¹⁹F *T*₁ relaxation times. For the four samples with resolved ¹⁹F isotropic chemical shifts, 2D ¹⁹F-¹⁹F exchange spectra were measured using the CORD ¹H irradiation scheme⁴⁹ during the mixing period. For sitagliptin, additional 2D spectra without ¹H irradiation during mixing, i.e., PDSD, were measured to compare the efficiency of spin exchange with and without ¹⁹F-¹H dipolar recoupling. The ¹H rf field strengths for CORD and DARR irradiation were calibrated independently to ensure correct adjustment and comparability between different experiments.

For SF-Trp, polarization transfer between magnetically inequivalent spins was measured using the CODEX experiment in the absence of molecular motion.^{53,50} CODEX decays were quantified by normalizing the intensity of the exchange spectrum, *S*(*t*_{mix}), to the intensity of the control spectrum, *S*₀. To maintain the same *T*₁ relaxation effects between *S* and *S*₀ experiments, a second mixing period serving as a longitudinal relaxation delay of duration *t*_z was added, where *t*_z + *t*_{mix} is the same between the *S* and *S*₀ experiments. ¹⁹F radiofrequency (rf) field strengths for 90° and 180° pulses were calibrated to a nutation frequency of 71.4 kHz. The ¹⁹F 180° pulses were optimized by maximizing the intensity of the refocused echo signal, which minimizes pulse imperfections during the CSA recoupling periods. The CSA recoupling duration, *Nτ_r*, where *τ_r* is the rotor period, was chosen on the basis of the ¹⁹F CSA, Δδ, which is 29.3 kHz for SF-Trp at 14.1 T, such that *Nτ_rΔδ* = 10–13.

Simulations of ¹⁹F Anisotropy Spin Exchange. The measured spin diffusion rate *k*_{SD} for SF-Trp in the absence of ¹H irradiation (Figure 1a,b) was simulated using the SPINEVOLUTION program.⁵¹ We considered the three closest ¹⁹F spins from three molecules (Figure 2a), together with their nine closest ¹H spins, giving a total of 12 spins in the simulation. Only one of the three spins (*F*₁) was given initial *z*-polarization to initiate detectable spin diffusion, whereas the *z*-magnetization *I*_z of its two closest neighbors (¹⁹F₂, ¹⁹F₃) was monitored as a function of mixing time. Due to symmetry, detecting $\langle I_{z,2}(t) + I_{z,3}(t) \rangle / 2$ is equivalent to detecting only $\langle I_{z,2}(t) \rangle$ or only $\langle I_{z,3}(t) \rangle$, because $\langle I_{z,2}(t) \rangle = \langle I_{z,3}(t) \rangle$ after powder averaging. We used 168 crystal orientations created using the REPULSION scheme for powder averaging.⁵² Only polarization transfer between ¹⁹F spins of different CSA tensor orientations results in CODEX signal decays. However, the presence of a third ¹⁹F spin (¹⁹F₃, with the same tensor orientation as ¹⁹F₂) facilitates polarization transfer and affects the MAS dependence of spin exchange.⁵³ The polarization buildup $\langle I_{z,2}(t) \rangle$ is independent of the actual starting configuration and detection scheme and can be approximated by $I_z(t) \approx Wt^2$, where *W* is the polarization transfer rate

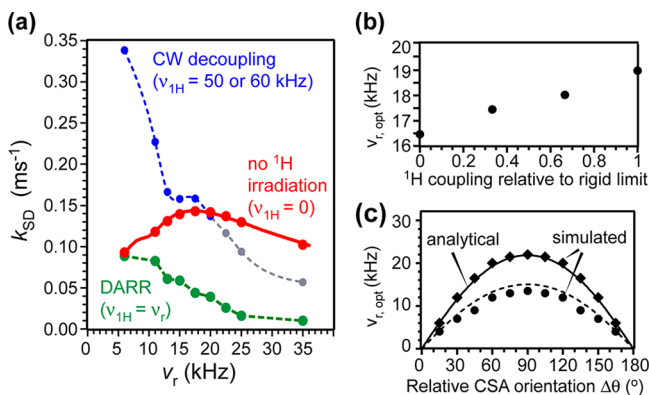


Figure 1. Dependence of ^{19}F spin exchange rates in SF-Trp on the MAS frequency ν_r at 564 MHz Larmor frequency. (a) Measured (points) MAS dependence of spin exchange rates without ^1H irradiation ($\nu_{1\text{H}} = 0$), with DARR irradiation ($\nu_{1\text{H}} = \nu_r$), and with strong ^1H CW decoupling ($\nu_{1\text{H}} \geq 50$ kHz). For MAS frequencies larger than 20 kHz, ^1H CW decoupling interferes with the $n = 2$ DARR condition and slows down ^{19}F spin exchange (gray circles). Dashed lines are guides to the eye, while the solid line for the ^1H -undecoupled data is from SPINEVOLUTION simulations using three ^{19}F spins and nine nearest protons (Figure 2a). (b) Optimal MAS frequency for ^1H undecoupled ^{19}F spin exchange, obtained from SPINEVOLUTION simulation, for different ^1H - ^1H and ^1H - ^{19}F dipolar couplings. (c) Numerical simulations (symbols) and analytical prediction (lines) of the optimal MAS frequency as a function of the angle $\Delta\theta$ between the two ^{19}F chemical-shift tensors. The upper curve corresponds to CSA parameters of $\Delta\delta = 75$ ppm and $\eta = 0.5$, while the lower curve corresponds to the SF-Trp CSA parameters of $\Delta\delta = 52$ ppm and $\eta = 0.04$.

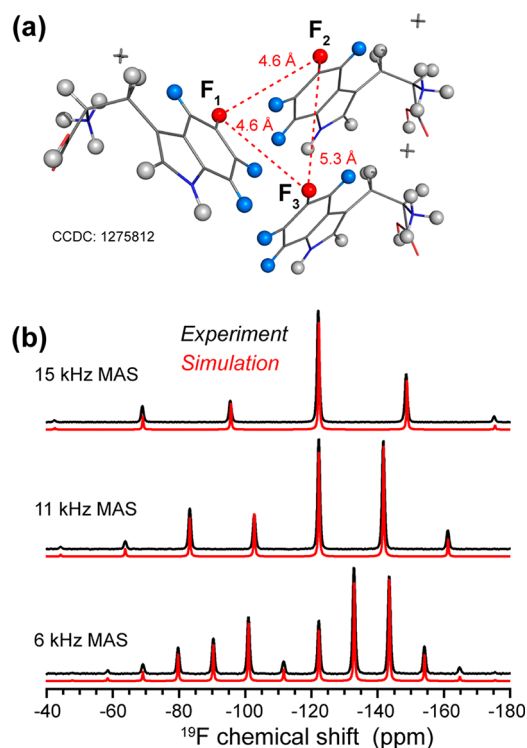


Figure 2. Crystal structure and ^{19}F spectrum of SF-Trp. (a) Crystal structure of hydrogenated L-Trp,⁶⁸ where HS has been replaced by ^{19}F (red). The upper two molecules belong to the same unit cell. Hydrogen atoms that were included in the ^{19}F spin exchange simulations are highlighted in blue. (b) Experimental (black) and simulated (red) ^{19}F spectrum of SF-Trp using SIMPSON and the parameters given in Table 1.

per unit time and is proportional to the spin diffusion rate k_{SD} with a proportionality constant that is shared among all simulations.⁵³ ^1H - ^{19}F and ^1H - ^1H dipolar coupling strengths were varied from zero to the rigid limit in the simulations to investigate the impact of ^1H dipolar couplings on the optimal MAS frequency under which spin diffusion is most efficient. For each dipolar scaling factor, the spin diffusion buildup curve was simulated as a function of MAS frequency, with the MAS frequency yielding the fastest buildup being identified in Figure 1b. The best-fit simulation for the ^1H -undecoupled spin exchange rates in Figure 1a used a ^1H dipolar scaling factor of 1/3 in the simulations, which approximates the fact that the actual (average) ^1H couplings to the ^{19}F spins are smaller than the couplings from the three closest protons to each ^{19}F used in the simulation. The value of 1/3 was determined by interpolating the impact of the ^1H - ^{19}F and ^1H - ^1H dipolar coupling strength based on simulations with and without the impact of protons, assuming a linear relationship between the ^1H dipolar coupling strength and the MAS frequency under which PDSD is the fastest. Additional simulations with a ^1H dipolar rescaling factor of 2/3 indicates that this assumption is justified (Figure 1b). In addition, effects of the ^{19}F CSA tensor orientation on ^{19}F - ^{19}F polarization transfer (Figure 1c) were simulated using the SIMPSON program,⁵⁴ considering only two ^{19}F spins and no ^1H .

RESULTS AND DISCUSSION

Spin Exchange between Chemically Equivalent ^{19}F Spins. We first investigated the optimal conditions for efficient CODEX anisotropy spin exchange at a magnetic field of 14.1 T, using SF-Trp as the model compound. SF-Trp has two inequivalent molecules in the asymmetric unit cell,³⁷ with a ^{19}F - ^{19}F distance of 4.6 Å and a relative orientation of 90° between the two C5-F5 bonds (Figure 2a). Spinning sideband spectra at 6, 11, and 15 kHz MAS (Figure 2b) indicate that the chemical-shift tensor has an anisotropy $\Delta\delta = \delta_{zz} - \delta_{\text{iso}}$ of 53.7 ± 0.8 ppm and an asymmetry parameter of $\eta = 0.04 \pm 0.08$, in agreement with literature.^{37,55} We measured the SF-Trp CODEX intensities as a function of MAS frequency (6 to 35 kHz) and ^1H irradiation field strength, $\nu_{1\text{H}}$ (0 to 60 kHz).

In the absence of motion, the CODEX experiment probes dipolar polarization transfer between spins with distinct instantaneous chemical shifts.^{35,36,56} Spin exchange among m magnetically inequivalent spins reduces the T_1 -compensated echo intensity S/S_0 to an equilibrium value of $1/m$ according to

$$\frac{S(t_{\text{mix}})}{S_0} = \left(1 - \frac{1}{m}\right) e^{-k_{\text{SD}} t_{\text{mix}}} + \frac{1}{m} \quad (1)$$

where the exponential decay rate, k_{SD} , depends on the distance-dependent dipolar coupling ω as^{37,57}

$$k_{\text{SD}} \approx 0.5\pi\omega^2 F(0) \quad (2)$$

Here, $F(0)$ is the overlap integral between the normalized zero-quantum line shapes $f_i(\omega - \omega_i)$ of the two spins and ω_i is the center of each peak,

$$F(0) = \int_{-\infty}^{+\infty} f_i(\omega - \omega_i) f_j(\omega - \omega_j) d\omega \quad (3)$$

The value of $F(0)$ is affected by ^{19}F - ^1H and ^1H - ^1H dipolar couplings, which impact the zero-quantum line shapes. Under MAS, ^{19}F - ^1H dipolar couplings are largely averaged out but can be reintroduced by ^1H continuous-wave (CW) irradiation at the $\nu_1 = \nu_R$ ($n = 1$) or $\nu_1 = 2\nu_R$ ($n = 2$) DARR condition.^{9,58}

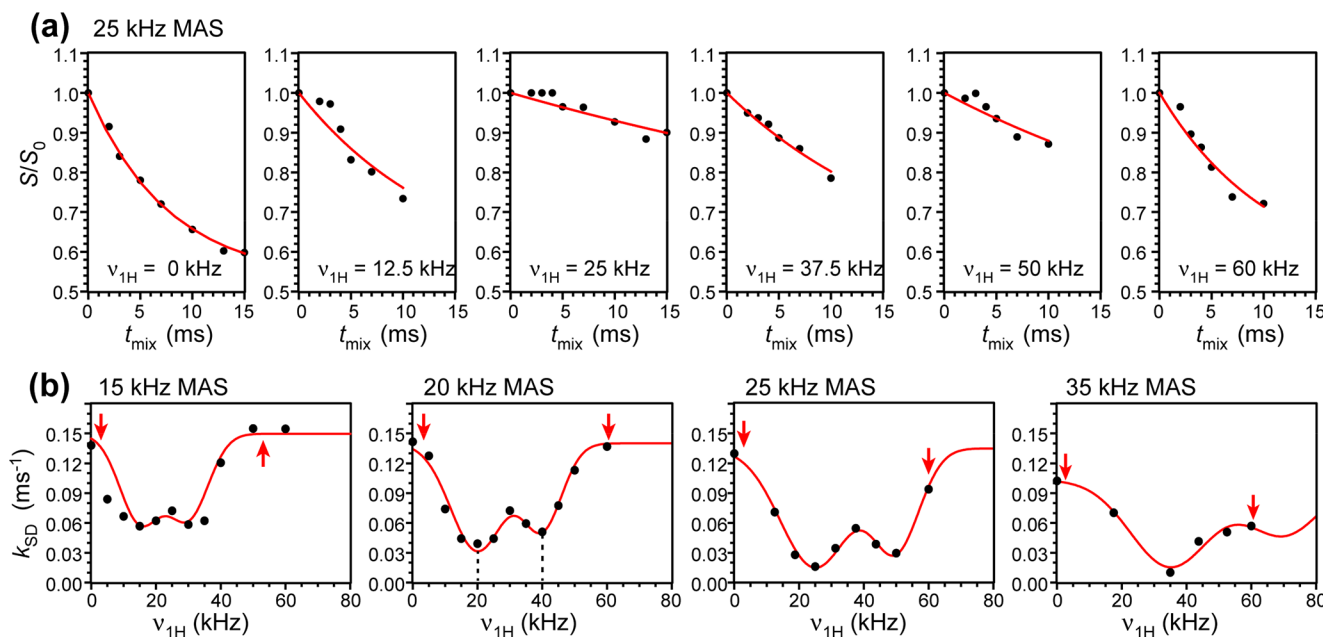


Figure 3. ^{19}F CODEX spin exchange data of SF-Trp. (a) CODEX decays (black) under 25 kHz MAS for different ^1H irradiation field strengths. Best fits (red) used an equilibrium value of 0.53 ± 0.03 , which was determined from the ^1H -undecoupled spin diffusion data. (b) Spin exchange rates k_{SD} (points) as a function of the ^1H irradiation field strength, $\nu_{^1\text{H}}$, for MAS frequencies of 15 to 35 kHz. Lines are sums of two Gaussian curves with fixed peak positions at $\nu_{^1\text{H}} = \nu_r$ and $\nu_{^1\text{H}} = 2\nu_r$. Arrows indicate lower- and upper-bound ^1H field strengths for which ^{19}F spin diffusion is the fastest.

Figure 3a shows CODEX decays of SF-Trp at 25 kHz MAS for different ^1H irradiation field strengths. The equilibrium S/S_0 value is, for different MAS rates, between 0.49 and 0.54, which is consistent with the unit cell structure. At the DARR conditions of $\nu_{^1\text{H}} = 25$ and 50 kHz, the CODEX echo intensities decay more slowly than other $\nu_{^1\text{H}}$ values, indicating that ^{19}F – ^1H dipolar recoupling slows down rather than speeds up spin exchange. Figure 3b plots the exchange rates k_{SD} as a function of $\nu_{^1\text{H}}$ for different MAS frequencies. At all MAS frequencies, ^{19}F spin exchange is *slower* under the DARR conditions than without ^1H irradiation (i.e., PDSD), with differences as much as 5-fold. This can be understood because ^1H – ^{19}F dipolar couplings experienced by the two ^{19}F spins differ; thus DARR recoupling reduces the overlap integral for these spins at the same ω_i or isotropic shift.^{53,59,60}

Figure 1a summarizes the observed joint dependence of k_{SD} on the MAS frequency and $\nu_{^1\text{H}}$. In addition to the slow exchange rates under the DARR condition, we observed interesting differences between spin exchange rates under strong ^1H decoupling and no ^1H decoupling. At slow MAS rates of less than 10 kHz, ^1H decoupling results in the fastest ^{19}F spin exchange. For example, at 6 kHz MAS, the polarization transfer rate is 3.5-fold faster with ^1H CW decoupling than without decoupling. As the MAS frequency increases to 15–20 kHz, which is 2–3 times the ^{19}F – ^1H dipolar coupling of 8.1 kHz for a 2.4 Å ^{19}F – ^1H distance, spin diffusion rates are similar with and without ^1H decoupling. At even faster MAS, ^1H decoupling slows down polarization transfer, probably because the decoupling fields of 50–60 kHz approach the $n = 2$ DARR condition. In this regime, undecoupled ^{19}F PDSD spin exchange is the most efficient. In the MAS range 6–35 kHz, ^1H -undecoupled ^{19}F spin exchange exhibits the highest exchange rates at MAS frequencies of 15–25 kHz, with a maximum at 17.5 kHz MAS.

The existence of an optimal MAS frequency for ^1H -undecoupled ^{19}F anisotropy spin exchange can be understood as a compromise between MAS-induced transient level crossings that speed up

spin exchange and reduction of ^{19}F – ^{19}F dipolar coupling by MAS. We can estimate this optimal frequency using the theory of rotor-driven polarization transfer,⁶¹ by considering the frequency required to match the average *instantaneous* chemical-shift difference between the two ^{19}F spins (Supporting Information):

$$\nu_{r,\text{opt}} \cong |\Delta\delta \cdot \sin \Delta\theta| \frac{\sqrt{(18 + \eta^2)(15 + \cos(2\Delta\theta))}}{8\sqrt{15}} \approx \frac{|\Delta\delta \cdot \sin \Delta\theta|}{2} \quad (4)$$

where $\Delta\delta$ is the chemical-shift anisotropy parameter in the unit of Hertz and $\Delta\theta$ is the angle between the largest chemical-shift principal axis of the two ^{19}F tensors. For SF-Trp (Table 1), $\Delta\theta = 90^\circ$; thus eq 4 predicts a $\nu_{r,\text{opt}}$ of 15.5 kHz, which is in reasonable agreement with the measured optimal MAS frequency of 17.5 kHz (Figure 1a). SPINEVOLUTION simulations (solid line in Figure 1a) using 33% scaled ^1H – ^{19}F and ^1H – ^1H dipolar couplings resulted in excellent agreement with the experimentally measured k_{SD} values as a function of MAS frequency. The scaling of ^{19}F – ^1H dipolar couplings is necessary because only the closest ^1H spins were used in the SPINEVOLUTION simulation while the average ^1H – ^{19}F dipolar coupling is weaker. Increasing ^{19}F – ^1H and ^1H – ^1H dipolar coupling shifts the optimal MAS frequency to larger values, as seen in Figure 1b.

Figure 1c compares the $\Delta\theta$ dependences of the optimal MAS frequency predicted from eq 4 and the simulated optimal MAS frequency using a simplified two-spin simulation. Good agreement is seen between the two. The optimal MAS frequency reaches a maximum when the two main principal axes of the CSA tensors are perpendicular to each other, consistent with eq 4.

We can express the dependence of ^{19}F spin diffusion rates on ^1H irradiation in terms of an effective ^{19}F overlap integral, $F_{\text{eff}}(0)$, which can be estimated as the ratio between the measured k_{SD} and the effective dipolar coupling, $\omega_{\text{eff}} = (\sum \omega_i^2)^{1/2}$, as $F_{\text{eff}}(0) \approx k_{\text{SD}}/0.5\pi\omega_{\text{eff}}^2$. For SF-Trp, ω_{eff} is $2\pi \cdot 2315$ Hz on the basis of

previously reported values.³⁷ The resulting $F_{\text{eff}}(0)$ values for SF-Trp from 6 to 35 kHz MAS under no ^1H irradiation, ^1H DARR irradiation, and ^1H CW decoupling, are shown in Table 2.

Table 2. Effective Overlap Integral $F_{\text{eff}}(0)$ for 5- ^{19}F -Trp as a Function of MAS Frequency ν_r and ^1H Irradiation during the CODEX Mixing Time

ν_r (kHz)	$F_{\text{eff}}(0)$ (μs)		
	PDSD	DARR	CW decoupling
6	14	13	50
11	18	12	34
13	19	9	25
15	21	9	23
17.5	21	7	23
20	21	6	20
22.5	20	4	17
25	19	2	14
35	15	2	8

The values of the effective overlap integral show a moderate dependence on the MAS frequency and are lower than the value of 37 μs measured under 8 kHz MAS at 9.4 T,³⁷ which can be attributed to the higher magnetic field and larger chemical shift in the current study.

^{19}F Spin Exchange between Spins with Distinct Isotropic Chemical Shifts. We next turned to ^{19}F spin exchange between chemically distinct spins for measuring distances in multifluorinated proteins and pharmaceutical compounds. It is well-known that ^{13}C zero-quantum spin exchange is facilitated by ^1H irradiation at a field strength that matches the MAS frequency. Under this DARR or CORD condition, the recoupled ^1H - ^{13}C dipolar interaction speeds up ^{13}C spin diffusion. For ^{19}F spins, isotropic chemical-shift differences can be as large as 100 ppm, which should make DARR or CORD spin diffusion

very beneficial. However, these large chemical-shift differences can exceed ^{19}F - ^1H and ^1H - ^1H dipolar couplings, which may weaken the effect of ^1H - ^{19}F recoupling on spin diffusion. The large ^{19}F CSA may further complicate polarization transfer by reducing or enhancing the chemical-shift difference between the two spins. Thus, accounting for ^{19}F chemical shifts will be important for accurate distance measurements.

To investigate the dependence of ^{19}F spin exchange on internuclear distances, ^1H - ^{19}F dipolar couplings, and chemical-shift differences, we studied four multifluorinated compounds, including PNC, sitagliptin, formyl-MLF, and 3F-Tyr-GB1 (Figure 4-7). These compounds manifest a wide range of isotropic shift differences, from less than 1 ppm between GB1 tyrosine resonances to 80 ppm between CF_3 and aromatic fluorines in sitagliptin and formyl-MLF. Table 1 and Figure S2 summarize the ^{19}F chemical-shift tensors in these compounds.⁶² Peak assignment was based on well-known chemical-shift trends, the measured spin exchange time constants, and the intramolecular distances from the crystal structures. SIMPSON simulations (not shown) confirm that ^{19}F spin diffusion experiences rotor-driven polarization transfer with respect to the isotropic chemical-shift difference,⁶¹ which will not be discussed here. Instead, an MAS frequency of 25 kHz was kept constant in the following experiments, which avoids rotational resonance between peaks.

PNC contains three aromatic fluorines separated by 4.7–9.4 Å and have small ^{19}F isotropic shift differences of 5.8–14.6 ppm (Figure 4a,b, Table 1). Dilution by Trp caused a second set of chemical shifts, which are not analyzed here (Figure 4c). 2D ^{19}F - ^{19}F CORD spectra revealed spin exchange buildup constants of 16 to 68 ms (Figure 4d). Most buildup curves plateau to 0.33, indicating equilibration of the magnetization among the three fluorines without considerable dipolar truncation affecting the plateau value.¹⁷ Figure 4e summarizes the buildup time constants, $t_{\text{SD}} = 1/k_{\text{SD}}$, for the three-spin system. Shorter time

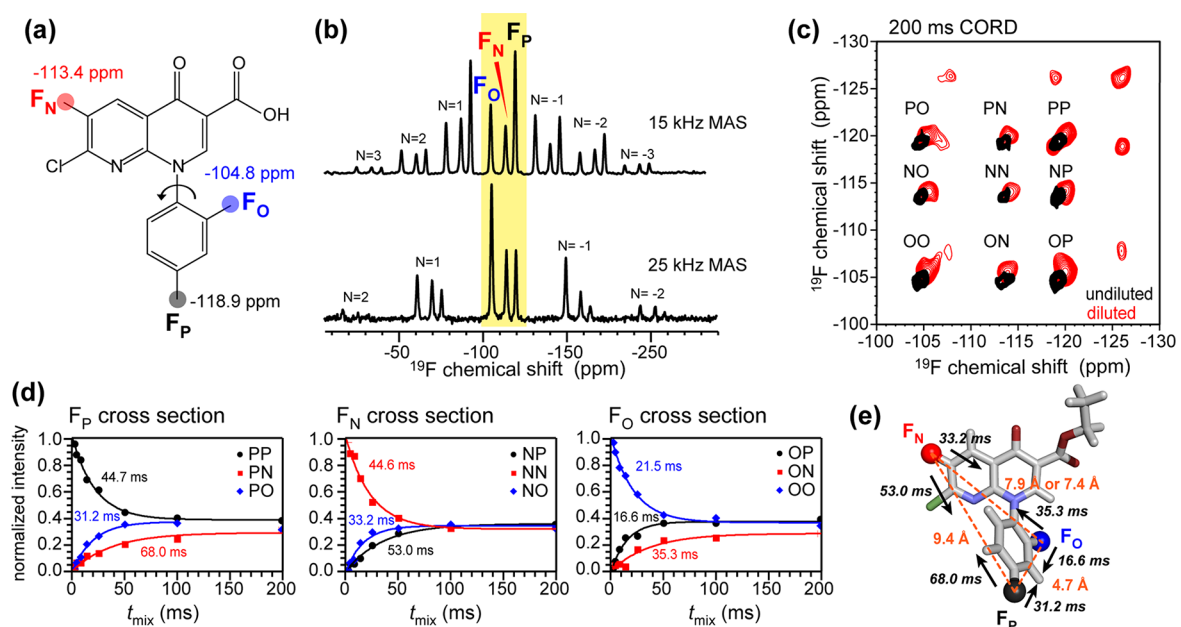


Figure 4. ^{19}F spin exchange of PNC. (a) Chemical structure of PNC, indicating the isotropic chemical shifts of the three fluorines. (b) ^{19}F CP spectrum at 15 kHz and 25 kHz MAS. Centerband peaks ($N = 0$) are shaded in yellow. Significant sideband intensities ($N \neq 0$) are seen at 15 kHz MAS. (c) 2D ^{19}F - ^{19}F correlation spectrum measured using 200 ms CORD for undiluted (black) and 1:5 diluted (red) PNC. Additional peaks in the diluted spectrum result from perturbation by the diluting compound Trp, and are not analyzed. (d) Normalized intensities of cross peaks and diagonal peaks as a function of mixing time. Best-fit exponential time constants $t_{\text{SD}} = 1/k_{\text{SD}}$ are indicated. (e) Polarization exchange time constants for the ^{19}F - ^{19}F distances in the molecular structure of PNC.

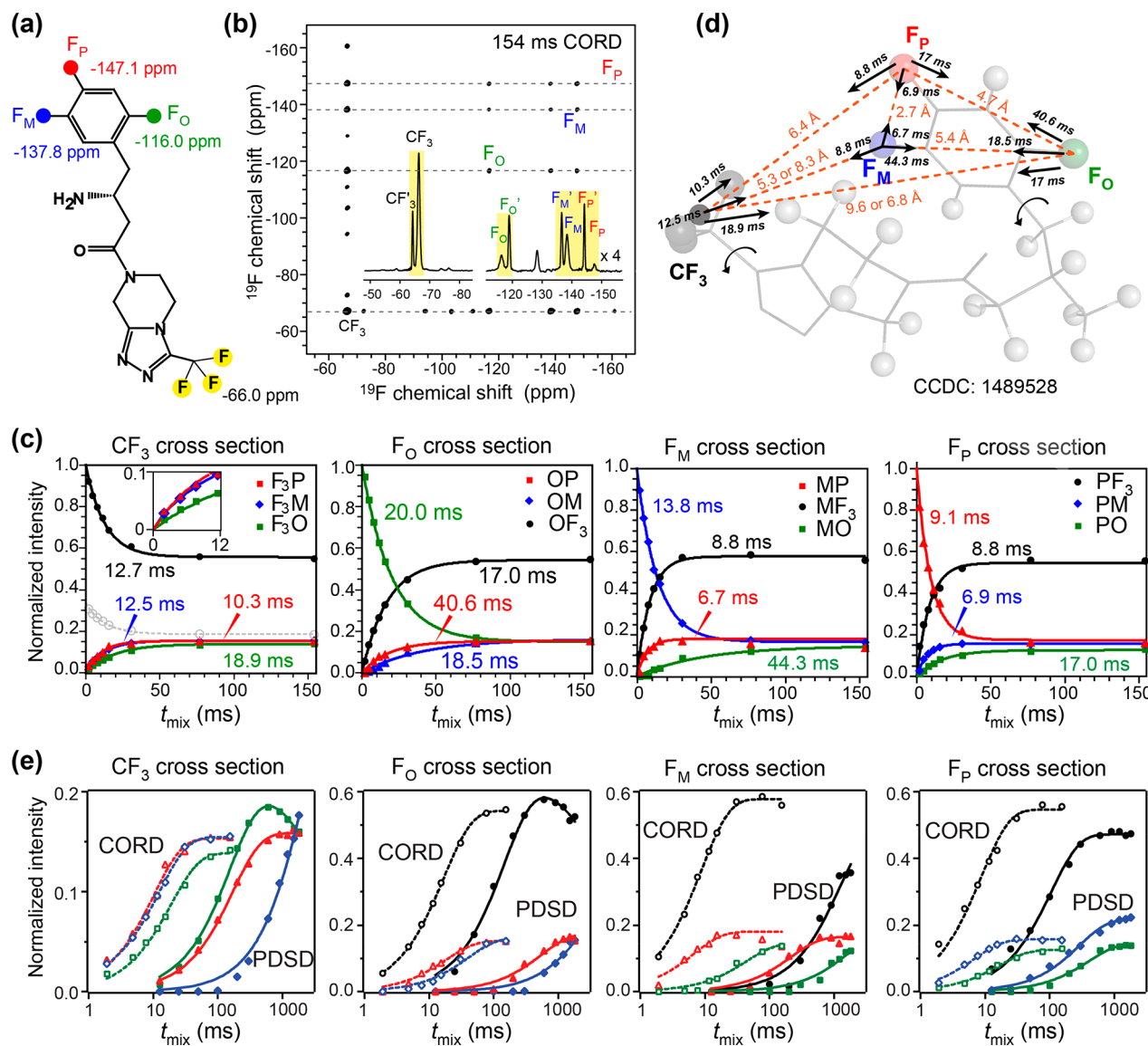


Figure 5. ¹⁹F spin exchange data of sitagliptin. (a) Chemical structure of sitagliptin and ¹⁹F isotropic chemical shifts. (b) 2D ¹⁹F-¹⁹F correlation spectrum of diluted sitagliptin, measured under 25 kHz MAS using 154 ms CORD mixing. Inset: ¹⁹F direct polarization spectrum at 35 kHz MAS. Assignment for the set of ¹⁹F signals that show correlation peaks is given. (c) Normalized intensities of cross peaks and diagonal peaks as a function of CORD mixing time. (d) Best-fit spin exchange time constants for the ¹⁹F-¹⁹F distances in sitagliptin.⁶⁹ Protons are shown as gray spheres. (e) Comparison of CORD (open symbols) and PDSD (filled symbols) ¹⁹F spin exchange buildup curves plotted on a logarithmic time axis. CORD spin exchange is much faster than PDSD. Intensity drops at long PDSD mixing times result from T_1 relaxation.

constants are found for shorter distances, as expected. Asymmetric time constants (16.6 and 31.2 ms) are observed between F_P and F_O, which are separated by 4.7 Å, which may result from complex multispin effects with the third ¹⁹F or with the different proton environments of the two fluorines.

Sitagliptin is an example of a fluorinated pharmaceutical compound: it is an FDA-approved antidiabetic compound containing a fluorinated β -amino acid linked to a trifluoromethyl-containing triazolopyrazine (Figure 5a). The trifluorophenyl ring enhances binding to a hydrophobic pocket of the target protein while the CF₃ group enhances activity by interacting electrostatically with the side chains of arginine and serine residues in the target protein.³⁴ Sitagliptin has large ¹⁹F isotropic chemical-shift differences of up to 80 ppm and inter-¹⁹F distances up to 9.6 Å. The 1D ¹⁹F spectrum resolves two sets of chemical shifts (Figure 5b), with the narrower set corresponding to a mobile population of molecules, as shown by the absence of their signals

in CP spectra (data not shown) and no associated cross-peaks in the 2D correlation spectra (Figure 5b). The spin exchange cross peaks of the rigid fraction of molecule show buildup time constants of 6.7–44.3 ms for distances of 4.7–9.6 Å (Figure 5c,d). Asymmetric spin exchange rates are again observed, for example, between F_M and F_O, with time constants of 44.3 and 18.5 ms. Here, we can attribute the slower F_M-to-F_O transfer to dipolar truncation, because F_M has a very short distance (2.7 Å) to F_P, while the F_O-F_P distance (4.7 Å) is considerably longer. Surprisingly, the CF₃ group, which is 5.3–9.6 Å away from the three aromatic fluorines, exhibits fast polarization transfer with time constants of 10–19 ms. The internuclear distances for the trifluoromethyl group were calculated as the average of the three individual distances, thus the three ¹⁹F spins are represented by a pseudospin located at the center of the three ¹⁹F spins. Accounting for each of the trifluoromethyl spins separately, and

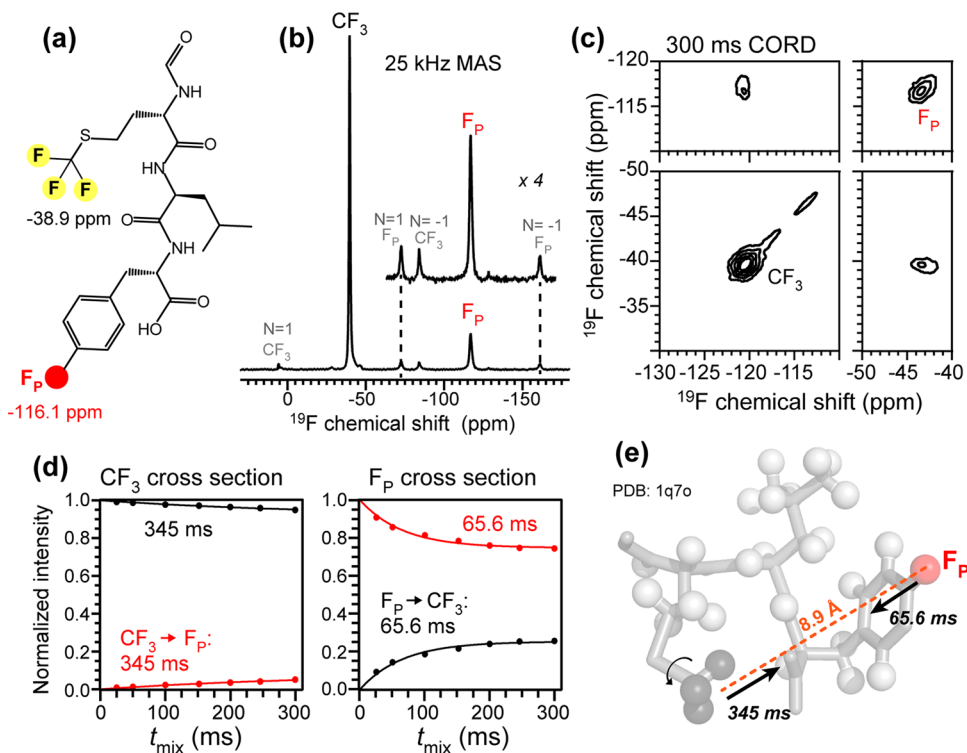


Figure 6. ^{19}F spin exchange of formyl-MLF. (a) Chemical structure and ^{19}F isotropic chemical shifts. (b) ^{19}F DP spectrum (black) at 25 kHz MAS. (c) 2D ^{19}F - ^{19}F correlation spectrum measured using 300 ms CORD mixing. (d) Normalized intensities of the cross peaks and diagonal peaks as a function of mixing time. (e) Spin exchange time constants for the ^{19}F - ^{19}F distance in formyl-MLF (PDB: 1q70⁷⁰).

considering that spin exchange rates scale with r^{-6} , yield the average internuclear distance as

$$\langle r \rangle = \left(\left(\sum_{i=1}^3 r^{-6} \right) / 3 \right)^{-1/6} \quad (5)$$

The resulting distances are close to those representing the trifluoromethyl group by a pseudospin, thus making the conclusions independent of the model used. In the pseudospin model, dipolar couplings with the trifluoromethyl group are simplified to a two-spin system experiencing an increased effective coupling strength.

To better understand the spin exchange trends between CF_3 and aromatic fluorines, we also measured ^{19}F - ^{19}F spin exchange in the tripeptide formyl-MLF (Figure 6). Compared to distances for sitagliptin, the CF_3 distance to $4\text{-}^{19}\text{F-Phe}$ is relatively long, at 8.9 Å. A time constant of 345 ms is observed from CF_3 to F_p , while the F_p -to- CF_3 transfer is much faster, with a time constant of 65.6 ms. This substantial asymmetry can be understood in terms of the effects of methyl rotation on intramethyl ^{19}F - ^{19}F dipolar coupling versus the CF_3 - CF dipolar coupling. For the long distance considered here, the trifluoromethyl rotation does not significantly affect the relative orientations of the three F_p - CF_3 vectors; thus polarization transfer from F_p to CF_3 is largely unaffected by motion. At the same time, ^{19}F - ^{19}F dipolar couplings among the three methyl fluorines are only reduced 2-fold from the rigid limit, giving a 5 kHz averaged dipolar coupling. This coupling truncates the coupling with the remote F_p spin, thus slowing down polarization transfer. Therefore, both the time constant and the plateau amplitude of spin exchange are highly directional in this spin system.

Fluorinated GB1 provides a realistic case of intramolecular ^{19}F spin exchange in proteins, where multiple residues of the

same type are incorporated. Figure 7a shows the positions of the three Tyr residues in GB1 (PDB: 2LGI)^{63,64}. Because the 3- ^{19}F and 5- ^{19}F positions are statistically equally present, there are eight isotopomers of Tyr-fluorinated GB1. However, because the distances involved are long, from 9 to 16 Å, the distance variation due to the 3- and 5-mixing does not significantly alter the distance distribution. Therefore, we use the coupling-weighted average of the 3F and 5F distances (eq 5) in our analysis. Parts b and c of Figure 7 show that Y3 and Y45 isotropic chemical shifts are significantly overlapped (0.4 ppm difference), while Y33 is resolved by 2–3 ppm from the other two peaks (Table 1). We thus analyzed the spin exchange rates between Y3 and Y45 by spectral deconvolution to reproduce the shape and position of the peak (Figure 7d). Y3–Y45 polarization transfer across a distance of 5.3 Å occurs with time constants of 37 and 81 ms and is manifested as near-diagonal intensities between the two closely spaced peaks. In comparison, Y45 and Y3 transfer to the resolved Y33 exhibit time constants of about 170 and 530 ms, corresponding to distances of 15.6 and 16.0 Å, respectively.

The 2D ^{19}F - ^{19}F exchange spectra in Figure 4–7 were measured under 25 kHz MAS using the CORD mixing scheme, with a maximum mixing time of 300 ms. When no ^1H irradiation was applied, the exchange rates slowed down more than 10-fold (Figure 5e, Figure S3). For sitagliptin, mixing times as long as 1.8 s were still insufficient for PDSD to reach equilibrium, and experiments with longer mixing times suffer from considerable T_1 relaxation. Even when the intensities are normalized to the integrated intensity of diagonal and cross peaks to compensate for the overall signal loss, several peaks show relaxation effects due to the large spread of relaxation times between the CF_3 and aromatic fluorines. For spin diffusion rates that are not significantly faster than T_1 relaxation, T_1 relaxation interferes with spin diffusion by causing local magnetization

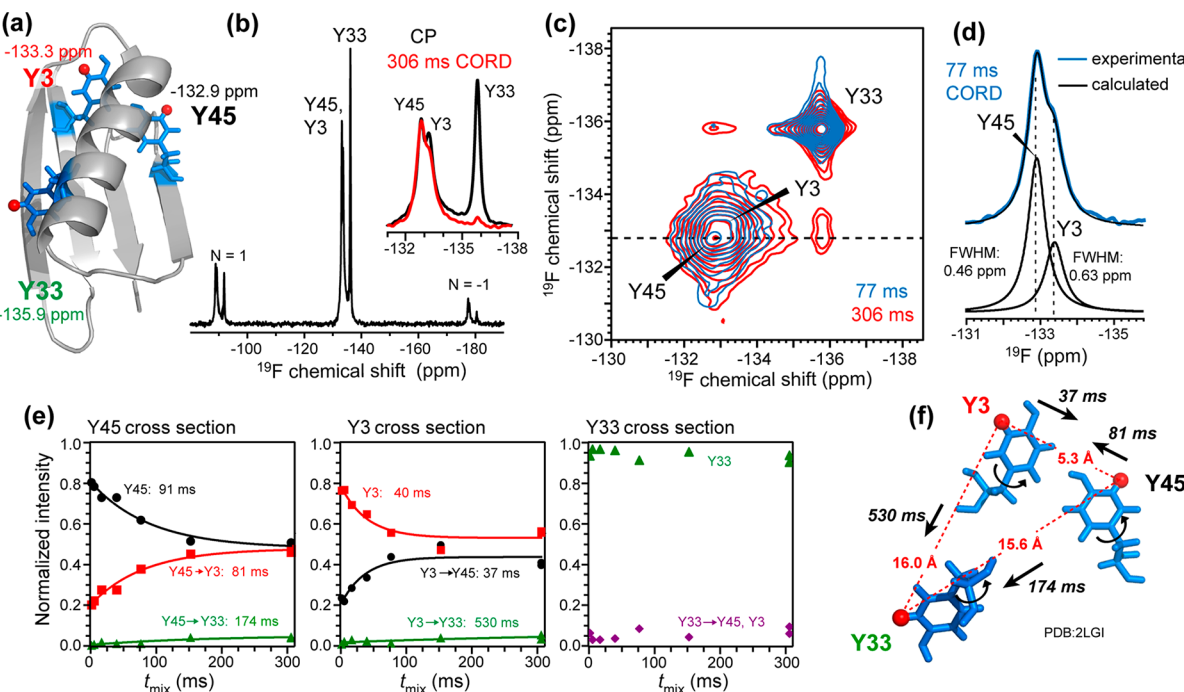


Figure 7. ^{19}F spin exchange of 3F-Tyr-GB1. (a) GB1 structure (PDB: 2JSV⁶³) and the ^{19}F isotropic chemical shifts. (b) ^{19}F CP spectrum at 25 kHz MAS. Inset: isotropic peaks from the ^{19}F CP spectrum (black) overlaid with the Y45 cross section (-132.9 ppm) of the 306 ms 2D CORD spectrum (red). (c) 2D ^{19}F - ^{19}F correlation spectra with 77 ms (blue) and 306 ms (red) mixing. (d) Peak deconvolution of Y45 and Y3. (e) Normalized intensities of cross peaks and diagonal peaks as a function of mixing time. (f) ^{19}F spin exchange time constants of the three ^{19}F sites for the ^{19}F - ^{19}F distances in GB1. The distances are the average distances for 3- ^{19}F and 5- ^{19}F positions.

gradients, leading to altered relaxation characteristics^{65,66} and biases to the cross-peak buildup curves. Therefore, CORD irradiation has significant benefit over PDSD for spectrally resolved ^{19}F spin exchange, in contrast to the dependence of CODEX anisotropy spin exchange among spins with the same isotropic shift.

Master Curve for Distance-Dependent ^{19}F Spin Exchange Rates. Given the large ranges of interfluorine distances and ^{19}F chemical shifts in these model compounds, we asked whether a simple quantitative relationship exists between spin diffusion rates and distances. For spin pairs for which phenyl ring reorientation introduces multiple distances, mean distances were calculated by the r^{-6} -weighted average according to eq 5. We note that phenyl ring reorientations are much faster than the characteristic spin polarization exchange times, giving a single, average distance for each spin pair. Though PNC and sitagliptin structures already include the fluorinated sites, F-F distances in formyl-MLF and GB1 were determined from their nonfluorinated analogues. Given the large F-F distances in these compounds, minor structural distortions due to fluorination are considered negligible. A simple plot of k_{SD} values with distances did not reveal a clear correlation with internuclear distances (Figure 8, inset), which is not surprising because the ^{19}F chemical shifts exert a strong influence on the spin exchange rates. We note that for ^1H spin diffusion under 100 kHz MAS, where ^1H resonances become narrow enough to avoid resonance overlap, similar bias effects were obtained: cross-peak intensities after a fixed ^1H spin diffusion period without dipolar recoupling correlate with the chemical-shift offset between the ^1H resonances.⁶⁷ This situation stresses the strong effects of chemical-shift bias even for systems in which isotropic chemical-shift differences are small, provided that (residual) dipolar couplings are smaller than the chemical-shift offsets.

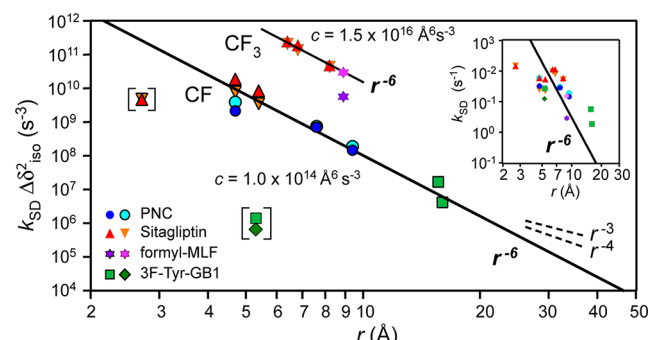


Figure 8. Chemical-shift modified spin exchange rates as a function of ^{19}F - ^{19}F distances. Two buildup rates are observed per spin pair. Solid lines have a slope of -6 to indicate the $1/r^6$ dependence; cf. eq 7. CF-CF spin exchange has a distinct and smaller proportionality constant c than CF-CF₃ spin exchange, but both show the $1/r^6$ dependence. Data points in brackets are expected outliers to which the chemical-shift correction does not apply; see main text and Supporting Information.

Because the spin diffusion rate is proportional to the overlap integral (eq 2), which is inversely proportional to the square of the isotropic shift difference (Supporting Information), we next scaled the k_{SD} values by the squared isotropic shift difference within each spin pair. This treatment is equivalent to approximating the overlap integral as

$$F(0) \approx f_0 / \Delta\delta_{\text{iso}}^2 \quad (6)$$

where f_0 is a phenomenological constant. With this approximation, the spin diffusion rate can be expressed as

$$k_{\text{SD}} \Delta\delta_{\text{iso}}^2 = 0.5\pi f_0 \omega^2 = \frac{c}{r^6} \quad (7)$$

where the constant c depends on f_0 , the ^{19}F gyromagnetic ratio, and the (powder averaged) orientation between the internuclear vector and the magnetic field. On a logarithmic scale, this chemical-shift modified rate then scales with distance r as

$$\log(k_{\text{SD}}\Delta\delta_{\text{iso}}^2) = \log c - 6 \log r \quad (8)$$

Figure 8 shows a logarithmic plot of $k_{\text{SD}}\Delta\delta_{\text{iso}}^2$ with respect to the distance r . Most data points fall onto two straight lines with the predicted slope of -6 , indicating data consistency and accuracy. Interestingly, the data points for the lower line correspond to CF–CF spin exchange while the data points for the upper line represent CF_3 –CF exchange. The calibration constant for the CF–CF exchange curve corresponds to $c = 1.0 \cdot 10^{14} \text{ \AA}^6/\text{s}^3$, whereas for CF_3 –CF exchange, the data indicate a 100-fold larger c of $1.5 \cdot 10^{16} \text{ \AA}^6/\text{s}^3$. Evidently, methyl rotational averaging of the ^{19}F CSA and simultaneous polarization transfer of three fluorines to a remote fluorine (or vice versa) significantly speeds up spin diffusion.

The approximation used here to compensate for chemical-shift bias, eq 7, does not apply to overlapped peaks or to spin pairs in the strong-coupling limit (Supporting Information). Thus, two outliers are expected and indeed observed using this approach. The partially overlapped Y3 and Y45 resonances in GB1 exhibit much slower spin diffusion rates than predicted by eq 7, which is fully consistent with the behavior of anisotropy spin exchange under ^1H irradiation. In the limit of negligible isotropic shift differences (strong coupling limit), ^{19}F spin exchange is significantly impeded by DARR or CORD ^1H – ^{19}F dipolar recoupling. The second outlier belongs to the 2.7 \AA F_M – F_P distance in sitagliptin, whose associated ^{19}F – ^{19}F dipolar coupling strength ($2\pi \cdot 5.4 \text{ kHz}$) is comparable to the isotropic shift difference of $2\pi \cdot 5.25 \text{ kHz}$. Therefore, this two-spin system also exists in the strong coupling limit, for which CORD recoupling impedes spin diffusion in a manner similar to that observed for 5F-Trp. Using $F_{\text{eff}}(0) = 2 \mu\text{s}$ under 25 kHz MAS and DARR irradiation (Table 2), and replacing the square of the angular dependence of dipolar couplings by its isotropic average of 0.2 , the internuclear distance is calculated to be 2.4 \AA , which matches the expected internuclear distance well. Therefore, the master curves apply to spin systems only in the weak-coupling limit, where the ^{19}F chemical-shift differences exceed the ^{19}F – ^{19}F dipolar couplings. This is the limit where we expect to find most applications of ^{19}F NMR for structure determination, particularly when measuring long distances.

These two master curves are obtained from compounds with ^{19}F – ^{19}F distances of 4.5 – 16 \AA and ^{19}F isotropic chemical shifts of -39 to -138 ppm , reflecting a broad range of chemical structures. Therefore, the observation that the chemical-shift corrected spin exchange rates not only exhibit a rigorous dependence on $1/r^6$ but also converge to a precise constant c means that spin exchange rates can be used to determine interfluorine distances reliably. The ability to measure distances up to 1.6 nm without exogenous paramagnetic or fluorescent tags should significantly facilitate biomolecular structure determination. We note that the longest distance examined in this study was measured under considerable dipolar truncation, which causes low cross peak intensities. In the absence of dipolar truncation, distances up to $\sim 2 \text{ nm}$ may be measurable. The asymmetry in polarization transfer does not compromise distance extraction, because the faster spin exchange rate within a pair of fluorines represents the more accurate distance.

CONCLUSIONS

The above ^{19}F spin exchange data provide the first extensive and quantitative measurement of ^{19}F – ^{19}F distances at a relatively high magnetic field of 14.1 T under fast MAS and take into account ^{19}F chemical-shift bias. Even with the simple spin diffusion mechanism, distances up to 1.6 nm were measured within a mixing time of 300 ms , making ^{19}F spin exchange NMR a robust method for obtaining long-range distance constraints. For distances of 6 – 8 \AA , ^{19}F – ^{19}F spin exchange time constants of 10 – 35 ms were found, which are 2 orders of magnitude faster than ^{13}C – ^{13}C spin exchange. ^{19}F spin exchange is efficient both between spins with the same isotropic chemical shift and between spins with different isotropic shifts. For the former case, anisotropy spin exchange is the most efficient under 15 – 25 kHz MAS, without ^1H irradiation, whereas DARR is detrimental. At even higher magnetic fields, the larger ^{19}F CSA will further increase the MAS frequency regime for efficient spin exchange. In contrast, spectrally resolved ^{19}F spin diffusion is facilitated by ^1H – ^{19}F dipolar recoupling. We discovered two master curves for CF–CF and CF – CF_3 spin exchange, which relate the measured exchange rates with distances after taking into account isotropic chemical-shift differences. Therefore, ^{19}F spin exchange NMR is a simple and robust approach for accurate distance measurements of ^{19}F – ^{19}F distances in a wide range of molecular systems with high sensitivity.

ASSOCIATED CONTENT

Supporting Information

The Supporting Information is available free of charge on the ACS Publications website at DOI: [10.1021/acs.jpcb.8b00310](https://doi.org/10.1021/acs.jpcb.8b00310).

Method for deriving the optimal MAS frequency for CODEX anisotropy spin exchange, motivation for, and limitations of, the chemical-shift bias correction, comparison of the spin exchange buildup time constants for PDSD and CORD experiments, line shape of solid-state NMR resonances, representative ^{19}F sideband spectra for extracting the ^{19}F CSA, ^{19}F PDSD buildup curves for sitagliptin (PDF)

AUTHOR INFORMATION

Corresponding Author

*Mei Hong. E-mail: meihong@mit.edu.

ORCID

Matthias Roos: [0000-0001-7062-7851](https://orcid.org/0000-0001-7062-7851)

Tuo Wang: [0000-0002-1801-924X](https://orcid.org/0000-0002-1801-924X)

Alexander A. Shcherbakov: [0000-0002-5728-7175](https://orcid.org/0000-0002-5728-7175)

Mei Hong: [0000-0001-5255-5858](https://orcid.org/0000-0001-5255-5858)

Present Address

[†]Department of Chemistry, Louisiana State University, Baton Rouge, LA 70803.

Notes

The authors declare no competing financial interest.

ACKNOWLEDGMENTS

This work is supported by NIH grant GM066976 to M. H. and by a Leopoldina postdoctoral fellowship (grant number LPDS-2017-14) from the German National Academy of Science to M. R. The authors thank Mikaila Hoffmann for help with the analysis of the spin exchange data.

■ REFERENCES

(1) Hong, M.; Schmidt-Rohr, K. Magic-Angle-Spinning NMR techniques for measuring long-range distances in biological macromolecules. *Acc. Chem. Res.* **2013**, *46*, 2154–2163.

(2) De Paëpe, G. Dipolar recoupling in magic angle spinning solid-state nuclear magnetic resonance. *Annu. Rev. Phys. Chem.* **2012**, *63*, 661–684.

(3) Saalwächter, K. Robust NMR approaches for the determination of homonuclear dipole–dipole coupling constants in studies of solid materials and biomolecules. *ChemPhysChem* **2013**, *14*, 3000–3014.

(4) Saalwächter, K.; Schnell, I. REDOR-based heteronuclear dipolar correlation experiments in multi-spin systems: rotor-encoding, directing, and multiple distance and angle determination. *Solid State Nucl. Magn. Reson.* **2002**, *22*, 154–187.

(5) Lange, A.; Seidel, K.; Verdier, L.; Luca, S.; Baldus, M. Analysis of proton–proton transfer dynamics in rotating solids and their use for 3D structure determination. *J. Am. Chem. Soc.* **2003**, *125*, 12640–12648.

(6) Castellani, F.; vanRossum, B.; Diehl, A.; Schubert, M.; Rehbein, K.; Oschkinat, H. Structure of a protein determined by solid-state magic-angle spinning NMR spectroscopy. *Nature* **2002**, *420*, 98–102.

(7) Wang, T.; Williams, J. K.; Schmidt-Rohr, K.; Hong, M. Relaxation-compensated difference spin diffusion NMR for detecting ¹³C-¹³C long-range correlations in proteins and polysaccharides. *J. Biomol. NMR* **2015**, *61*, 97–107.

(8) Szeverenyi, N. M.; Sullivan, M. J.; Maciel, G. E. Observation of spin exchange by Two-Dimensional Fourier Transform ¹³C Cross Polarization-Magic-Angle Spinning. *J. Magn. Reson.* **1982**, *47*, 462–475.

(9) Takegoshi, K.; Nakamura, S.; Terao, T. ¹³C-¹H dipolar-assisted rotational resonance in magic-angle spinning NMR. *Chem. Phys. Lett.* **2001**, *344*, 631–637.

(10) Morcombe, C. R.; Gaponenko, V.; Byrd, R. A.; Zilm, K. W. Diluting abundant spins by isotope edited radio frequency field assisted diffusion. *J. Am. Chem. Soc.* **2004**, *126*, 7196–7197.

(11) De Paëpe, G.; Lewandowski, J. R.; Loquet, A.; Böckmann, A.; Griffin, R. G. Proton assisted recoupling and protein structure determination. *J. Chem. Phys.* **2008**, *129*, 245101.

(12) Hu, B.; Lafon, O.; Trébosc, J.; Chen, Q.; Amoureaux, J. P. Broadband homo-nuclear correlations assisted by ¹H irradiation for biomolecules in very high magnetic field at fast and ultra-fast MAS frequencies. *J. Magn. Reson.* **2011**, *212*, 320–329.

(13) Shen, M.; Liu, Q.; Trébosc, J.; Lafon, O.; Masuda, Y.; Takegoshi, K.; Amoureaux, J. P.; Hu, B.; Chen, Q. Exploring various modulation-sideband recoupling conditions of SHA+ sequence at fast MAS. *Solid State Nucl. Magn. Reson.* **2013**, *55–56*, 42–47.

(14) Weingarth, M.; Demco, D. E.; Bodenhausen, G.; Tekely, P. Improved magnetization transfer in solid-state NMR with fast magic angle spinning. *Chem. Phys. Lett.* **2009**, *469*, 342–348.

(15) Hou, G.; Yan, S.; Trébosc, J.; Amoureaux, J.-P.; Polenova, T. Broadband homonuclear correlation spectroscopy driven by combined R2_n sequences under fast magic angle spinning for NMR structural analysis of organic and biological solids. *J. Magn. Reson.* **2013**, *232*, 18–30.

(16) Hu, B.; Trébosc, J.; Lafon, O.; Chen, Q.; Masuda, Y.; Takegoshi, Y.; Amoureaux, J.-P. Very-long-distance correlations in proteins revealed by solid-state NMR spectroscopy. *ChemPhysChem* **2012**, *13*, 3585–3588.

(17) Bayro, M. J.; Huber, M.; Ramachandran, R.; Davenport, T. C.; Meier, B. H.; Ernst, M.; Griffin, R. G. Dipolar truncation effect in magic-angle spinning NMR recoupling experiments. *J. Chem. Phys.* **2009**, *130*, 114506.

(18) Ni, Q. Z.; Daviso, E.; Can, T. V.; Markhasin, E.; Jawla, S. K.; Swager, T. M.; Temkin, R. J.; Herzfeld, J.; Griffin, R. G. High Frequency Dynamic Nuclear Polarization. *Acc. Chem. Res.* **2013**, *46*, 1933–1941.

(19) Gullion, T.; Schaefer, J. Rotational echo double resonance NMR. *J. Magn. Reson.* **1989**, *81*, 196–200.

(20) Kristiansen, P. E.; Caravetta, M.; van Beek, J. D.; Lai, W. C.; Levitt, M. H. Theory and applications of supercycled symmetry-based recoupling sequences in solid-state nuclear magnetic resonance. *J. Chem. Phys.* **2006**, *124*, 234510.

(21) Solomon, I. Relaxation processes in a system of two spins. *Phys. Rev.* **1955**, *99*, 559–565.

(22) Nadaud, P. S.; Helmus, J. J.; Kall, S. L.; Jaroniec, C. P. Paramagnetic ions enable tuning of nuclear relaxation rates and provide long-range structural restraints in solid-state NMR of proteins. *J. Am. Chem. Soc.* **2009**, *131*, 8108–8120.

(23) Nadaud, P. S.; Helmus, J. J.; Sengupta, I.; Jaroniec, C. P. Rapid Acquisition of Multidimensional Solid-State NMR Spectra of Proteins Facilitated by Covalently Bound Paramagnetic Tags. *J. Am. Chem. Soc.* **2010**, *132*, 9561–9563.

(24) Buffy, J. J.; Hong, T.; Yamaguchi, S.; Waring, A.; Lehrer, R. I.; Hong, M. Solid-State NMR Investigation of the Depth of Insertion of Protegin-1 in Lipid Bilayers Using Paramagnetic Mn²⁺. *Biophys. J.* **2003**, *85*, 2363–2373.

(25) Su, Y.; Hu, F.; Hong, M. Paramagnetic Cu(II) for Probing Membrane Protein Structure and Function: Inhibition Mechanism of the Influenza M2 Proton Channel. *J. Am. Chem. Soc.* **2012**, *134*, 8693–8702.

(26) Wang, T.; Chen, Y.; Tabuchi, A.; Cosgrove, D. J.; Hong, M. The Target of β -Expansin EXPB1 in Maize Cell Walls from Binding and Solid-State NMR Studies. *Plant Physiol.* **2016**, *172*, 2107–2119.

(27) Pintacuda, G.; Giraud, N.; Pierattelli, R.; Böckmann, A.; Bertini, I.; Emsley, L. Solid-state NMR spectroscopy of a paramagnetic protein: assignment and study of human dimeric oxidized CuII-ZnII superoxide dismutase (SOD). *Angew. Chem., Int. Ed.* **2007**, *46*, 1079–1082.

(28) Gregory, D. H.; Gerig, J. T. Structural effects of fluorine substitution in proteins. *J. Comput. Chem.* **1991**, *12*, 180–185.

(29) Merkel, L.; Schauer, M.; Antranikian, G.; Budisa, N. Parallel incorporation of different fluorinated amino acids: on the way to “teflon” proteins. *ChemBioChem* **2010**, *11*, 1505–1507.

(30) Salwiczek, M.; Nyakatura, E. K.; Gerling, U. I. M.; Ye, S.; Koksch, B. Fluorinated amino acids: compatibility with native protein structures and effects on protein–protein interactions. *Chem. Soc. Rev.* **2012**, *41*, 2135–2171.

(31) Matei, E.; Gronenborn, A. M. (19)F Paramagnetic Relaxation Enhancement: A Valuable Tool for Distance Measurements in Proteins. *Angew. Chem., Int. Ed.* **2016**, *55*, 150–154.

(32) Eddy, M. T.; Didenko, T.; Stevens, R. C.; Wüthrich, K. β 2-Adrenergic Receptor Conformational Response to Fusion Protein in the Third Intracellular Loop. *Structure* **2016**, *24*, 2190–2197.

(33) Manglik, A.; Kim, T. H.; Masureel, M.; Altenbach, C.; Yang, Z.; Hilger, D.; Lerch, M. T.; Kobilka, T. S.; Thian, F. S.; Hubbell, W. L.; Prosser, R. S.; Kobilka, B. K. Structural Insights into the Dynamic Process of β 2-Adrenergic Receptor Signaling. *Cell* **2015**, *161*, 1101–1111.

(34) Wang, J.; Sánchez-Roselló, M.; Aceña, J. L.; del Pozo, C.; Sorochinsky, A. E.; Fustero, S.; Soloshonok, V. A.; Liu, H. Fluorine in pharmaceutical industry: fluorine-containing drugs introduced to the market in the last decade (2001–2011). *Chem. Rev.* **2014**, *114*, 2432–2506.

(35) deAzevedo, E. R.; Bonagamba, T. J.; Hu, W.; Schmidt-Rohr, K. Centerband-only detection of exchange: efficient analysis of dynamics in solids by NMR. *J. Am. Chem. Soc.* **1999**, *121*, 8411–8412.

(36) Buffy, J. J.; Waring, A. J.; Hong, M. Determination of peptide oligomerization in lipid membranes with magic-angle spinning spin diffusion NMR. *J. Am. Chem. Soc.* **2005**, *127*, 4477–4483.

(37) Luo, W.; Hong, M. Determination of the Oligomeric Number and Intermolecular Distances of Membrane Protein Assemblies by Anisotropic ¹H-Driven Spin Diffusion NMR Spectroscopy. *J. Am. Chem. Soc.* **2006**, *128*, 7242–7451.

(38) Luo, W.; Mani, R.; Hong, M. Sidechain conformation and gating of the M2 transmembrane peptide proton channel of influenza A virus from solid-state NMR. *J. Phys. Chem. B* **2007**, *111*, 10825–10832.

(39) Williams, J. K.; Zhang, Y.; Schmidt-Rohr, K.; Hong, M. pH-Dependent Conformation, Dynamics, and Aromatic Interaction of the

Gating Tryptophan Residue of the Influenza M2 Proton Channel from Solid-State NMR. *Biophys. J.* **2013**, *104*, 1698–1708.

(40) Mandala, V. S.; Liao, S. Y.; Kwon, B.; Hong, M. Structural Basis for Asymmetric Conductance of the Influenza M2 Proton Channel Investigated by Solid-State NMR Spectroscopy. *J. Mol. Biol.* **2017**, *429*, 2192–2210.

(41) Williams, J. K.; Shcherbakov, A. A.; Wang, J.; Hong, M. Protonation equilibria and pore-opening structure of the dual-histidine influenza B virus M2 transmembrane proton channel from solid-state NMR. *J. Biol. Chem.* **2017**, *292*, 17876–17884.

(42) Salnikov, E. S.; Raya, J.; De Zotti, M.; Zaitseva, E.; Peggion, C.; Ballano, G.; Toniolo, C.; Raap, J.; Bechinger, B. Alamethicin Supramolecular Organization in Lipid Membranes from ¹⁹F Solid-State NMR. *Biophys. J.* **2016**, *111*, 2450–2459.

(43) Gilchrist, J. M. L.; Monde, K.; Tomita, Y.; Iwashita, T.; Nakanishi, K.; McDermott, A. E. Measurement of interfluorine distances in solids. *J. Magn. Reson.* **2001**, *152*, 1–6.

(44) Chen, Q.; Schmidt-Rohr, K. F-19 and C-13 NMR signal assignment and analysis in a perfluorinated ionomer (Nafion) by two-dimensional solid-state NMR. *Macromolecules* **2004**, *37*, 5995–6003.

(45) Martineau, C.; Legein, C.; Buzare, J.-Y.; Fayonc, F. On the assignment of ¹⁹F MAS NMR spectra of fluoroaluminates using through-space spectral edition of ¹⁹F–²⁷Al and ¹⁹F–¹⁹F connectivities. *Phys. Chem. Chem. Phys.* **2009**, *11*, 950–957.

(46) Wang, Q.; Hu, B.; Fayon, F.; Trébosc, J.; Legein, C.; Lafon, O.; Deng, F.; Amoureaux, J.-P. Double-quantum ¹⁹F-¹⁹F dipolar recoupling at ultra-fast magic angle spinning NMR: application to the assignment of ¹⁹F NMR spectra of inorganic fluorides. *Phys. Chem. Chem. Phys.* **2009**, *11*, 10391–10395.

(47) Wang, Q.; Hu, B.; Lafon, O.; Trébosc, J.; Deng, F.; Amoureaux, J.-P. Homonuclear dipolar recoupling under ultra-fast magic-angle spinning: Probing ¹⁹F–¹⁹F proximities by solid-state NMR. *J. Magn. Reson.* **2010**, *203*, 113–128.

(48) Langer, B.; Schnell, I.; Spiess, H. W.; Grimmer, A. R. Temperature calibration under ultrafast MAS conditions. *J. Magn. Reson.* **1999**, *138*, 182–186.

(49) Hou, G.; Yan, S.; Trébosc, J.; Amoureaux, J.-P.; Polenova, T. Broadband homonuclear correlation spectroscopy driven by combined R2_n sequences under fast magic angle spinning for NMR structural analysis of organic and biological solids. *J. Magn. Reson.* **2013**, *232*, 18–30.

(50) deAzevedo, E. R.; Kennedy, S. B.; Hong, M. Determination of slow motions in extensively isotopically labeled proteins by magic-angle-spinning ¹³C-detected ¹⁵N exchange NMR. *Chem. Phys. Lett.* **2000**, *321*, 43–48.

(51) Veshtort, M.; Griffin, R. G. SPINEVOLUTION: a powerful tool for the simulation of solid and liquid state NMR experiments. *J. Magn. Reson.* **2006**, *178*, 248–82.

(52) Bak, M.; Nielsen, N. C. REPULSION, A Novel Approach to Efficient Powder Averaging in Solid-State NMR. *J. Magn. Reson.* **1997**, *125*, 132–139.

(53) Roos, M.; Micke, P.; Saalwächter, K.; Hempel, G. Moderate MAS enhances local ¹H spin exchange and spin diffusion. *J. Magn. Reson.* **2015**, *260*, 28–37.

(54) Bak, M.; Rasmussen, J. T.; Nielsen, N. C. SIMPSON: A general simulation program for solid-state NMR spectroscopy. *J. Magn. Reson.* **2000**, *147*, 296–330.

(55) Dürr, H. N.; Grage, S. L.; Witter, R.; Ulrich, A. S. Solid state ¹⁹F NMR parameters of fluorine-labeled amino acids. Part I: Aromatic substituents. *J. Magn. Reson.* **2008**, *191*, 7–15.

(56) deAzevedo, E. R.; Bonagamba, T. J.; Hu, W.; Schmidt-Rohr, K. Principle of centerband-only detection of the exchange and extension to a four-time CODEX. *J. Chem. Phys.* **2000**, *112*, 8988–9001.

(57) Schmidt-Rohr, K.; Spiess, H. W. *Multidimensional solid-state NMR and polymers*; Academic Press Inc.: London, 1994.

(58) Oas, T. G.; Griffin, R. G.; Levitt, M. H. Rotary resonance recoupling of dipolar interactions in solid-state nuclear magnetic resonance spectroscopy. *J. Chem. Phys.* **1988**, *89*, 692–695.

(59) Roos, M.; Micke, P.; Hempel, G. Monitoring nuclear spin-flip processes and measuring spin-diffusion constants via hole burning into the magnetization. *Chem. Phys. Lett.* **2012**, *536*, 147–154.

(60) Chen, Q.; Schmidt-Rohr, K. Measurement of the local ¹H spin-diffusion coefficient in polymers. *Solid State Nucl. Magn. Reson.* **2006**, *29*, 142–152.

(61) Colombo, M. G.; Meier, B. H.; Ernst, R. R. Rotor-driven spin diffusion in natural-abundance ¹³C spin systems. *Chem. Phys. Lett.* **1988**, *146*, 189–196.

(62) Eichele, K. *HBA 1.7.5*, Universität Tübingen, 2015.

(63) Franks, W.; Wylie, B. J.; Frericks, H. L.; Nieuwkoop, A. J.; Mayrhofer, R.; Shah, G. H.; Graesser, D. T.; Rienstra, C. M. Dipole tensor-based refinement for atomic-resolution structure determination of a nanocrystalline protein by solid-state NMR spectroscopy. *Proc. Natl. Acad. Sci. U. S. A.* **2008**, *105*, 4621–4626.

(64) Wylie, B. J.; Sperling, L. J.; Nieuwkoop, A. J.; Franks, W. T.; Oldfield, E.; Rienstra, C. M. Ultrahigh resolution protein structures using NMR chemical shift tensors. *Proc. Natl. Acad. Sci. U. S. A.* **2011**, *108*, 16974–16979.

(65) Kalk, A.; Berendsen, H. C. J. Proton magnetic relaxation and spin diffusion in proteins. *J. Magn. Reson.* **1976**, *24*, 343–366.

(66) Roos, M.; Hofmann, M.; Link, S.; Ott, M.; Balbach, J.; Rössler, E.; Saalwächter, K.; Krushelnitsky, A. The “long tail” of the protein tumbling correlation function: observation by ¹H NMR relaxometry in a wide frequency and concentration range. *J. Biomol. NMR* **2015**, *63*, 403–415.

(67) Wittmann, J. J.; Agarwal, V.; Hellwagner, J.; Lends, A.; Cadalbert, R.; Meier, B. H.; Ernst, M. Accelerating proton spin diffusion in perdeuterated proteins at 100 kHz MAS. *J. Biomol. NMR* **2016**, *66*, 233–242.

(68) Takigawa, T.; Ashida, T.; Sasada, Y.; Kakudo, M. The crystal structures of L-tryptophan hydrochloride and hydrobromide. *Bull. Chem. Soc. Jpn.* **1966**, *39*, 2369–2378.

(69) Kaduk, J. A.; Zhong, K.; Gindhart, A. M.; Blanton, T. N. Crystal structure of sitagliptin dihydrogen phosphate monohydrate, C₁₆H₁₆F₆N₅O(H₂PO₄)(H₂O). *Powder Diffr.* **2015**, *30*, 349–356.

(70) Rienstra, C. M.; Tucker-Kellogg, L.; Jaroniec, C. P.; Hohwy, M.; Reif, B.; McMahon, M. T.; Tidor, B.; Lozano-Perez, T.; Griffin, R. G. *De novo* determination of peptide structure with solid-state magic-angle spinning NMR spectroscopy. *Proc. Natl. Acad. Sci. U. S. A.* **2002**, *99*, 10260–10265.